SCIENTIFIC REPORTS

OPEN

SUBJECT AREAS:
PHYSICS
MATERIALS SCIENCE
NANOSCIENCE AND TECHNOLOGY

Received
26 June 2014

Accepted
23 September 2014

Published
21 October 2014

Correspondence and requests for materials should be addressed to U.S. (udo.schwingenschlogl@kaust.edu.sa)

* Current address: Superconductivity and New Energy R&D Center, Key Laboratory of Advanced Technology of Materials (Ministry of Education), Southwest Jiaotong University, Chengdu, 610031, China

Order-disorder phase transitions in the two-dimensional semiconducting transition metal dichalcogenide alloys $Mo_{1-x}W_xX_2$ (X = S, Se, and Te)

Li-Yong Gan[1]*, Qingyun Zhang[1], Yu-Jun Zhao[2], Yingchun Cheng[1] & Udo Schwingenschlögl[1]

[1]PSE Division, KAUST, Thuwal 23955-6900, Kingdom of Saudi Arabia, [2]Department of Physics, South China University of Technology, Guangzhou 510640, People's Republic of China.

A combination of density functional theory, an empirical model, and Monte Carlo simulations is used to shed light on the evolution of the atomic distribution in the two-dimensional semiconducting transition metal dichalcogenide alloys $Mo_{1-x}W_xX_2$ (X = S, Se, and Te) as a function of the W concentration and temperature. Both random and ordered phases are discovered and the origin of the phase transitions is clarified. While the empirical model predicts at $x = 1/3$ and 2/3 ordered alloys, Monte Carlo simulations suggest that they only exist at low temperature due to a small energetic preference of Mo-X-W over Mo-X-Mo and W-X-W interactions, explaining the experimental observation of random alloy $Mo_{1-x}W_xS_2$. Negative formation energies point to a high miscibility. Tunability of the band edges and band gaps by alteration of the W concentration gives rise to a broad range of applications.

Two-dimensional materials often exhibit unique features, distinctly different from those of their bulk counterparts, and thus are receiving tremendous attention[1–3]. In particular, monolayers of semiconducting transition metal dichalcogenides, such as MoS_2 and WS_2, have versatile electronic[4–8], optical[9–11], mechanical[12–14], and chemical[15–17] properties, opening up new fundamental as well as technological avenues in a range of fields, including hydrogen evolution[15,16], transistors[18,19], energy storage[20,21], photodetectors[22], and electroluminescent devices[22,23]. However, there are still serious limitations related to the available band gap values. Alloying semiconductors is known to be an effective approach to achieve continuously tunable band gaps[24], as reported by both theory and experiment for anion mixing in $MoX_{2(1-x)}X'_{2x}$ alloys[25,26]. Recently, $Mo_{1-x}W_xS_2$ monolayers have been demonstrated experimentally[27,28] and it has been predicted that the band gap, hole/electron effective mass, ionization potential, and electron affinity can be engineered[29].

The atomic distribution in two-dimensional crystals is particularly critical for their practical use in nanodevices. Scanning transmission electron microscopy has revealed a random structure in $Mo_{1-x}W_xS_2$ alloys[27,28]. However, the samples were fabricated and characterized only at particular temperatures. It is important to know whether there exit any ordered alloys or, elsewise, what the physical origin of the random structure is. Furthermore, it is intriguing to clarify whether the possibility of alloying can be extended to other transition metal dichalcogenide monolayers. In the present work, density functional theory is combined with an empirical model and Monte Carlo simulations to systematically investigate the alloying behavior of semiconducting $Mo_{1-x}W_xX_2$ (X = S, Se, and Te) monolayers. Ordered alloys are identified at $x = 1/3$ and 2/3, but appear only at low temperature due to a small energetic preference of Mo-X-W over Mo-X-Mo and W-X-W interactions.

Results

First-principles calculations are performed using the Vienna Ab-initio Simulation Package and the Perdew-Burke-Ernzerhof generalized gradient approximation[30]. To derive parameters for the empirical model and Monte Carlo simulations, total energies are calculated in supercells containing 6×6 $Mo_{1-x}W_xX_2$ and a vacuum slab of 20 Å thickness. A cutoff energy of 500 eV and a Γ-centered $4 \times 4 \times 1$ k-mesh are used. The calculated lattice constants of MoX_2 and WX_2 are identical (3.18, 3.32, and 3.55 Å for X = S, Se, and Te, respectively), consistent with previous studies[31]. To compare the electronic structures, $\sqrt{3} \times \sqrt{3}$ supercells containing zero, one, two, and three W atoms and a vacuum slab of 20 Å thickness are used with a Γ-centered $15 \times 15 \times 1$ k-mesh. All

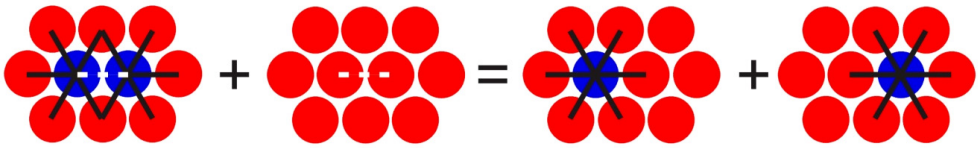

Figure 1 | Diagram illustrating the calculation of the energy gain due to the formation of Mo-X-W interactions from Mo-X-Mo and W-X-W interactions in $Mo_{1-x}W_xX_2$. Only Mo (red) and W (blue) atoms are shown. The Mo-X-W interactions are highlighted by black solid lines and the Mo-X-Mo as well as W-X-W interactions by white dashed lines.

the geometries are optimized until the residual forces remain below 0.01 eV/Å. Spin-orbit coupling is not considered, since its effect is much smaller than the variations of the band properties. The vacuum level is taken as reference point for the band edge.

The total energy (E_{tot}) of $Mo_{1-x}W_xX_2$ with n_{Mo} Mo and n_W W atoms is approximated by an empirical model based on the sum of M-X-M interactions, given by the energies $\varepsilon_{Mo\text{-}X\text{-}Mo}$, $\varepsilon_{Mo\text{-}X\text{-}W}$, and $\varepsilon_{W\text{-}X\text{-}W}$. The numbers of appearance of these interactions are denoted as $n_{Mo\text{-}X\text{-}Mo}$, $n_{Mo\text{-}X\text{-}W}$, and $n_{W\text{-}X\text{-}W}$. Then the total energy is given by

$$E_{tot} = \sum n_{Mo}\varepsilon_{Mo} + \sum n_W\varepsilon_W + \sum n_{Mo\text{-}X\text{-}Mo}\varepsilon_{Mo\text{-}X\text{-}Mo} + \sum n_{Mo\text{-}X\text{-}W}\varepsilon_{Mo\text{-}X\text{-}W} + \sum n_{W\text{-}X\text{-}W}\varepsilon_{W\text{-}X\text{-}W}. \quad (1)$$

The first two terms are atomic reference energies (ε_{Mo} and ε_W being the total energies of isolated Mo and W atoms, respectively), while the latter three refer to the three types of M-X-M interactions. The alloy formation energy at a W concentration of x is

$$E_f(x) = E_{tot} - (1-x)E(MoX_2) - xE(WX_2), \quad (2)$$

where $E(MoX_2)$ and $E(WX_2)$ are the total energies of MoX_2 and WX_2 per formula unit, respectively.

For a $Mo_{1-x}W_xX_2$ monolayer containing no W-X-W interaction the total energy depends only on x and not on the specific atomic distribution,

$$E_{ideal} = E_{MoX_2} + n_W\Delta E_W. \quad (3)$$

Here E_{MoX_2} is the total energy of a pristine MoX_2 monolayer, i.e., a supercell containing 6 × 6 MoX_2, and ΔE_W is the energy change encountered by substituting one W atom for one Mo atom in the limit $x \to 0$. In a random $Mo_{1-x}W_xX_2$ alloy with n W-X-W interactions, the energy deviates from E_{ideal} by

$$n\varepsilon = E_{tot} - E_{ideal}. \quad (4)$$

The energy gain due to the formation of one Mo-X-W interaction from Mo-X-Mo and W-X-W interactions is given by ε. According to Fig. 1, this can be expressed as

$$\varepsilon = 10\varepsilon_{Mo\text{-}X\text{-}W} + \varepsilon_{W\text{-}X\text{-}W} + \varepsilon_{Mo\text{-}X\text{-}Mo} - 12\varepsilon_{Mo\text{-}X\text{-}W} = \varepsilon_{W\text{-}X\text{-}W} + \varepsilon_{Mo\text{-}X\text{-}Mo} - 2\varepsilon_{Mo\text{-}X\text{-}W} \quad (5)$$

The probability for an exchange between two configurations is determined by the Boltzmann function, depending on the temperature T and the energy difference ΔE between the two configurations,

$$P = \frac{1}{1+\exp(\Delta E/k_BT)}. \quad (6)$$

When the number of W-X-W interactions changes by Δn we have

$$\Delta E = \Delta n\varepsilon. \quad (7)$$

We employ a 60 × 60 lattice with periodic boundary conditions for various values of ε/k_BT. A new atomic distribution is accepted if P exceeds a random number. This process is repeated up to 50 million times at each W concentration, which has been tested to yield the lowest energy structure.

For each $Mo_{1-x}W_xX_2$ alloy, density functional theory is used to calculate the total energies of 40 random configurations in a 6 × 6 supercell with different W concentrations between 0 and 1. Using Eq. (1) with the obtained total energies, the energy of the Mo-X-Mo, Mo-X-W, and W-X-W interactions in the empirical model are derived, see Table I. Subsequently, the total energies and corresponding formation energies of the random $Mo_{1-x}W_xX_2$ alloys are calculated. A comparison of the alloy formation energies derived by density functional theory and the model is displayed in Fig. 2(a). The agreement is excellent, confirming that it is sufficient to consider in the model only M-X-M interactions. According to Table I, the interaction energies decrease monotonously from S to Te due to the increasing M-M distance. The energy gain, due to the formation of a Mo-X-W interaction, derived from Eq. (5), is also given in Table I. The three positive values suggest that it is energetically favorable to form Mo-X-W interactions from Mo-X-Mo and W-X-W interactions. The formation energies as a function of the W concentration show similar behaviors for X = S, Se, and Te, see Figs. 2(b)–(d), respectively. The negative values suggest that miscible alloys are formed. Two ordered alloys are obtained at x = 1/3 and 2/3, for which the number of Mo-X-W interactions is maximized (W-X-W interactions are avoided). Both show a $\sqrt{3} \times \sqrt{3}\,R30^\circ$ superstructure, where the formation energies of the two ordered phases are the same.

Total energies calculated by density functional theory are used to derive ε from Eq. (4). The almost perfectly linear dependence for the three data sets in Fig. 3(a) suggests that M-X-M interactions are sufficient to accurately describe ε. We thus consider only those in our Monte Carlo simulations. We obtain for ε values of 6.9, 5.1, and 3.5 meV for X = S, Se, and Te, respectively, which agree well with the results derived from Eq. (1). The small values can be attributed to the identical lattices of MoX_2 and WX_2 and the chemical similarity of Mo and W. The elongated M-M distance results in a reduction of ε, pointing to the possibility of manipulating the value by strain.

Monte Carlo simulations are performed to explore how the atomic distribution evolves as a function of the temperature. The concentration of W monomers is defined as ratio between the number of W monomers and the total number of metal atoms. The results in Fig. 3(b) show that the W monomer concentration increases at any given $x < 0.50$ as the temperature decreases (ε/k_BT increases). Gradually, a peak develops at x = 1/3 around $\varepsilon/k_BT = 2.50$, suggest-

Table I | Mo-X-Mo ($\varepsilon_{Mo\text{-}X\text{-}Mo}$), Mo-X-W ($\varepsilon_{Mo\text{-}X\text{-}W}$), and W-X-W ($\varepsilon_{W\text{-}X\text{-}W}$) interaction energies derived from Eq. (1) and corresponding energy gain (ε) due to the formation of Mo-X-W interactions from Mo-X-Mo and W-X-W interactions in $Mo_{1-x}W_xX_2$ according to Eq. (5)

	$\varepsilon_{Mo\text{-}X\text{-}Mo}$ (meV)	$\varepsilon_{Mo\text{-}X\text{-}W}$ (meV)	$\varepsilon_{W\text{-}X\text{-}W}$ (meV)	ε (meV)
$Mo_{1-x}W_xS_2$	−5735.4	−6067.4	−6392.1	7.1
$Mo_{1-x}W_xSe_2$	−5118.2	−5412.1	−5700.9	5.1
$Mo_{1-x}W_xTe_2$	−4481.1	−4732.4	−4980.1	3.6

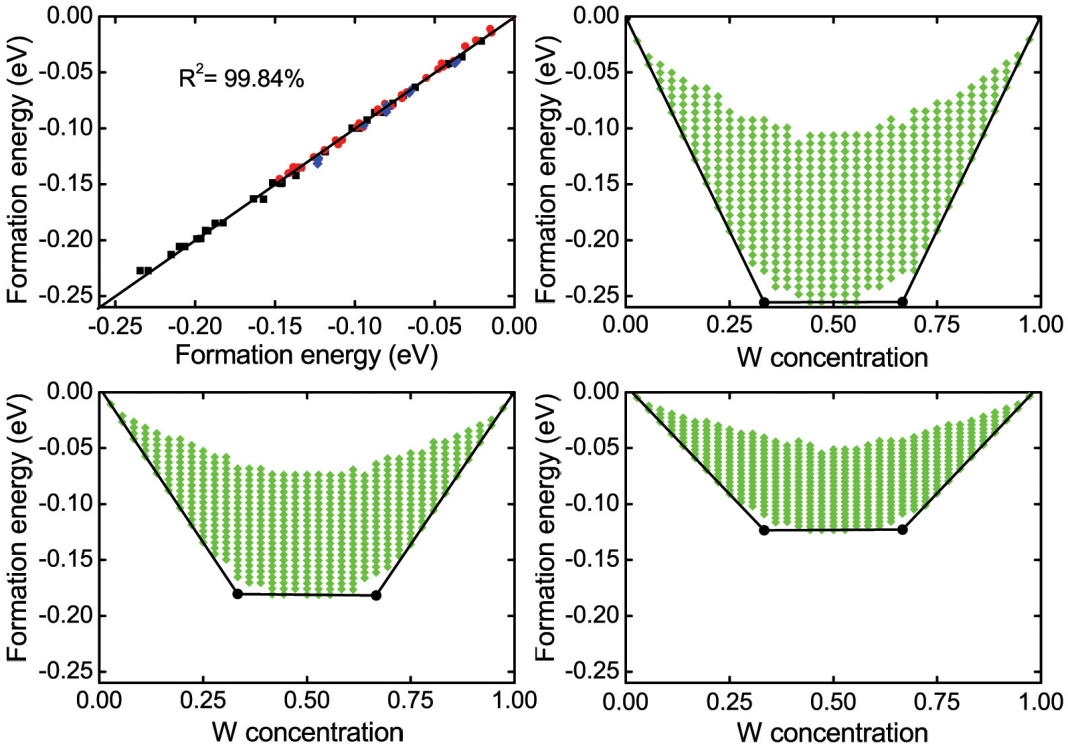

Figure 2 | (a) Comparison of the formation energies for $Mo_{1-x}W_xS_2$ (black squares), $Mo_{1-x}W_xSe_2$ (red dots), and $Mo_{1-x}W_xTe_2$ (blue diamonds) between density functional theory and the empirical model described by Eq. (1). Formation energies for (b) $Mo_{1-x}W_xS_2$, (c) $Mo_{1-x}W_xSe_2$, and (d) $Mo_{1-x}W_xTe_2$ as a function of the W concentration as predicted by 7 million random configurations. Black dots indicate the ordered alloys.

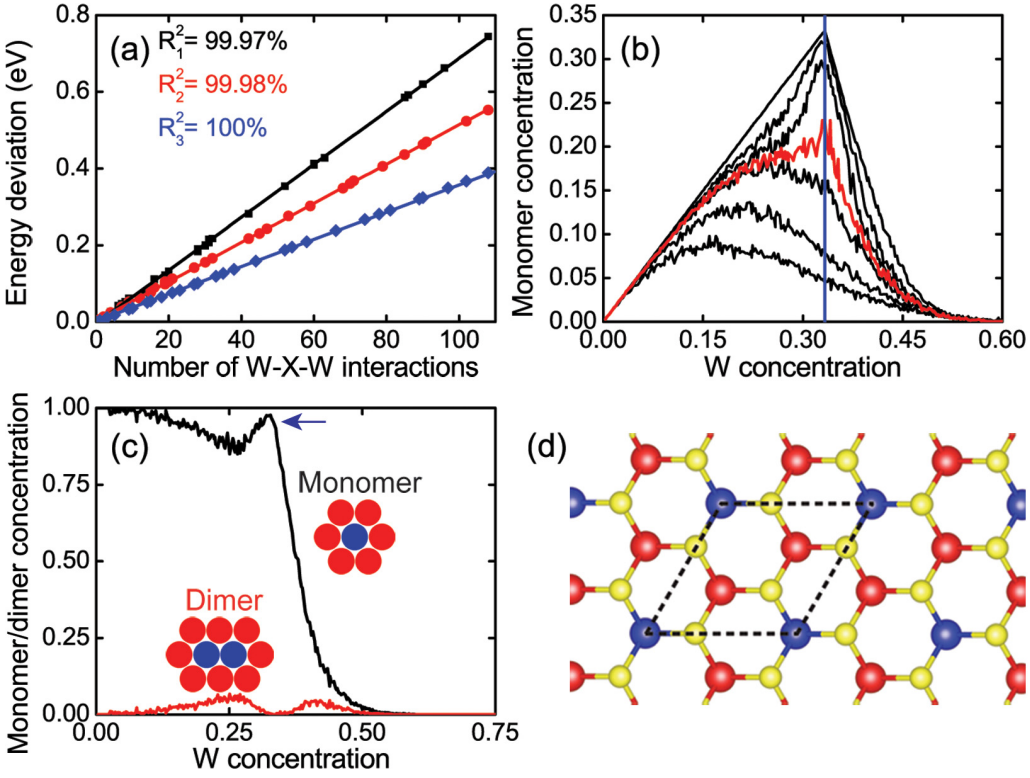

Figure 3 | (a) Energy deviation for $Mo_{1-x}W_xS_2$ (black squares), $Mo_{1-x}W_xSe_2$ (red dots), and $Mo_{1-x}W_xTe_2$ (blue diamonds) as a function of the number of W-X-W interactions. (b) Monomer concentration as a function of the W concentration (ratio between the number of W monomers and the total number of metal atoms) at selected values of $\varepsilon/k_BT = 0.217$, 1.25, 2.25, 2.5, 2.75, 3.25, and 7 (from bottom to top). The red line separates the random and ordered atomic distributions and the vertical blue line depicts $x = 1/3$. (c) W monomer/dimer concentration (ratio between the number of W monomers/dimers and the number of W atoms) as a function of the W concentration at $\varepsilon/k_BT = 2.75$. The insets show the structures without X atoms. (d) Top view on the structure of the configuration indicated by the arrow in (c). The unit cell is marked by dashed lines.

ing that an ordered structure is formed. This is ascribed to the fact that Mo-X-W interactions are energetically favorable over Mo-X-Mo and W-X-W interactions. The corresponding phase transition temperatures are estimated to be 36, 24, and 9 K for X = S, Se, and Te, respectively. At higher temperatures, in particular at room temperature, the small ε is insufficient to maximize the number of Mo-X-W interactions. Thus, random Mo/W distributions appear, rationalizing the observations of random $Mo_{1-x}W_xS_2$ alloys in recent experiments[27,28]. On the other hand, the sharp decrease of the W monomer concentration for $x > 1/3$ implies miscibility of the alloys. All three alloys under investigation share these properties.

Figure 3c shows the W monomer/dimer concentration (ratio between the number of W monomers/dimers and the number of W atoms) as function of x at $\varepsilon/k_BT = 2.75$. We find that the concentration of W monomers decreases when x increases from 0 to 0.26, while the concentration of W dimers increases. However, the concentration of dimers/monomers decreases/increase from $x = 0.25$ to 1/3. Eventually, the monomer concentration shows a peak and the dimer concentration approaches zero at $x = 1/3$, suggesting an ordered configuration. In fact we find that a $\sqrt{3} \times \sqrt{3}\,R30^\circ$ superstructure is formed, see Fig. 3(d), consistent with the model results. The curve can be understood by examining what happens when two adjacent Mo and W atoms are exchanged in a single Monte Carlo run. For small x, Δn tends to 1, giving a small probability that a new structure is accepted. Therefore, the W monomer concentration decreases. On the other hand, for $x \rightarrow 1/3$, Δn tends to 2, see the $\sqrt{3} \times \sqrt{3}\,R30^\circ$ configuration after exchanging two adjacent Mo and W atoms in Fig. 3(d), facilitating an ordering process. Increasing the W concentration beyond 1/3 sharply reduces the W monomer concentration, see Fig. 3(c), since every additional W atom will form W-X-W interactions. If the Mo monomer/dimer concentrations would be recorded, another $\sqrt{3} \times \sqrt{3}\,R30^\circ$ phase would be detected, in which the Mo and W atoms are exchanged ($x = 2/3$; red and blue color exchanged in Fig. 3(d)).

We next address the band gaps and band edges in the $Mo_{1-x}W_xX_2$ alloys, see Fig. 4, considering only the ordered states. Note that WTe_2 cannot be realized experimentally[32], suggesting limitations in W doping of $MoTe_2$. However, dilute doping should still be feasible. The band gap decreases from $x = 0$ to 1/3 and increases for $x > 1/3$, displaying a parabolic feature for both X = S and Se. The extended band gap range by alteration of the W concentration broadens the applicability of transition metal dichalcogenide monolayers in nano- and opto-electronics. Both the valence band maximum and conduction band minimum gradually shift to higher energy as x increases. Because the band edges mainly originate from metal d orbitals, the higher W 5d states result in a higher band edge. The valence band maximum shifts almost uniformly in all three alloys, whereas the conduction band minimum shifts hardly from $x = 0$ to 1/3 but remarkably for $x > 1/3$. Eventually, the magnitude of the latter shift exceeds that of the former, giving rise to a parabolic variation of the band gap. This feature can be understood by different compositions of the band edges in MoX_2 and WX_2[28,29]. Since the valence band maxima of MoX_2 and WX_2 originate from the metal d_{xy} and $d_{x^2-y^2}$ orbitals, doping a W atom in MoX_2 instantly shifts them up in

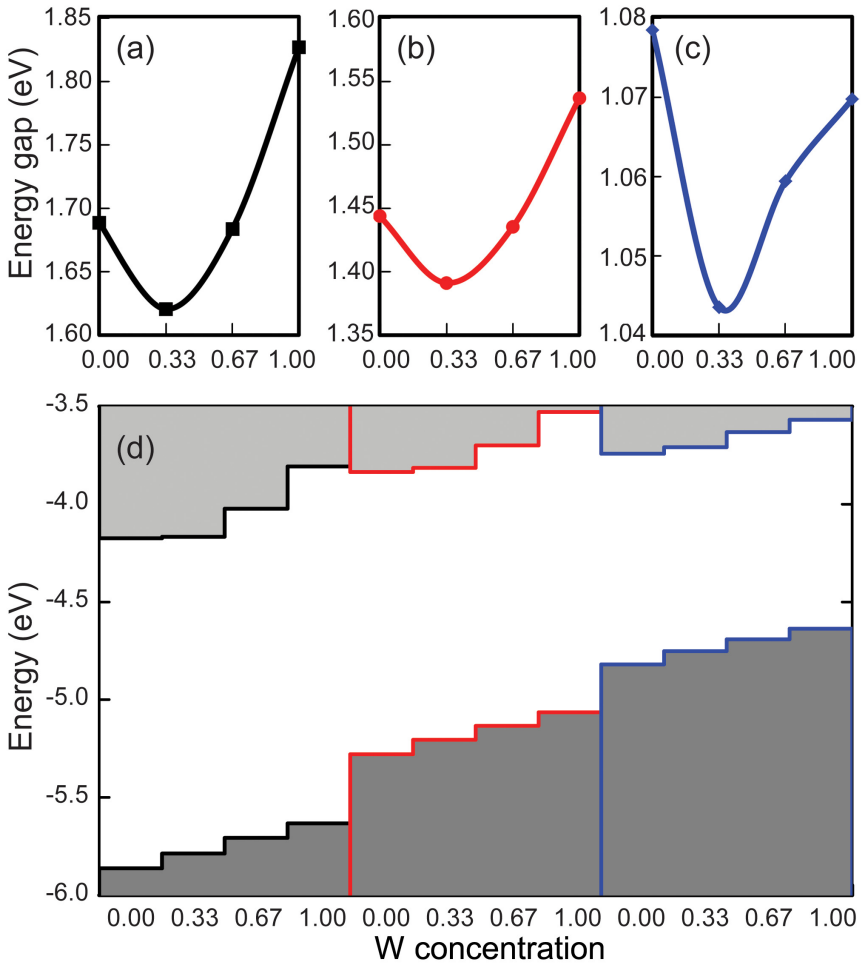

Figure 4 | Band gap variations for (a) $Mo_{1-x}W_xS_2$, (b) $Mo_{1-x}W_xSe_2$, and (c) $Mo_{1-x}W_xTe_2$ as a function of the W concentration. (d) Band alignment for the ordered states: $Mo_{1-x}W_xS_2$ (black), $Mo_{1-x}W_xSe_2$ (red), and $Mo_{1-x}W_xTe_2$ (blue).

energy. In contrast, the conduction band minimum is dominated by the metal $d_{3z^2-r^2}$ states in the case of MoX_2 but the d_{xy}, $d_{x^2-y^2}$, and $d_{3z^2-r^2}$ states in the case of WX_2. For $x < 1/3$, W contributes slightly to the conduction band minima, resulting in small energetic upshifts. For $x > 1/3$, the W contribution becomes dominant and thus the upshifts are enhanced. Furthermore, the M-X bond length increases from S to Te, which reduces the overlap between the M *d* and X *p* orbitals. Consequently, the magnitude of the band edge shift and of the band gap variation follows the order S > Se > Te.

Discussion

The atomic distributions in the two-dimensional semiconducting transition metal dichalcogenide $Mo_{1-x}W_xX_2$ (X = S, Se, and Te) alloys have been investigated by density functional theory, an empirical model, and Monte Carlo simulations. The ab-initio total energies have been used to parameterize the M-X-M interaction energies, yielding slight energetic preference of Mo-X-W over Mo-X-Mo and W-X-W interactions, which is ascribed to the identical MoX_2 and WX_2 lattices and the chemical similarity between Mo and W. Ordered alloys are predicted for $x = 1/3$ and 2/3 by the empirical model but only exist at low temperature according to the Monte Carlo simulations. At higher temperature the small energetic preference is not sufficient to maximize the number of Mo-X-W interactions, explaining the experimental observation of random $Mo_{1-x}W_xS_2$ alloys. Negative formation energies suggest a good miscibility for all three alloys. Our results demonstrate that the band gaps and band edges can be varied continuously in $Mo_{1-x}W_xX_2$ monolayers, with the minimal gap appearing around $x = 1/3$. The tunable band gap by alloying strongly broadens the range of possible applications of transition metal dichalcogenide monolayers.

1. Lee, C. *et al.* Frictional Characteristics of Atomically Thin Sheets. *Science* **328**, 76–80 (2010).
2. Schwierz, F. Graphene transistors. *Nat. Nanotech.* **5**, 487–496 (2010).
3. Britnell, L. *et al.* Field-Effect Tunneling Transistor Based on Vertical Graphene Heterostructures. *Science* **335**, 947–950 (2012).
4. Radisavljevic, B., Radenovic, A., Brivio, J., Giacometti, V. & Kis, A. Single-layer MoS_2 transistors. *Nat. Nanotech.* **6**, 147–150 (2011).
5. Zhu, Z. Y., Cheng, Y. C. & Schwingenschlögl, U. Giant Spin-Orbit-Induced Spin Splitting in Two-Dimensional Transition-Metal Dichalcogenide Semiconductors. *Phys. Rev. B* **84**, 153402 (2011).
6. Xiao, D., Liu, G.-B., Feng, W., Xu, X. & Yao, W. Coupled Spin and Valley Physics in Monolayers of MoS_2 and Other Group-VI Dichalcogenides. *Phys. Rev. Lett.* **108**, 196802 (2012).
7. Johari, P. & Shenoy, V. B. Tuning the Electronic Properties of Semiconducting Transition Metal Dichalcogenides by Applying Mechanical Strains. *ACS Nano* **6**, 5449–5456 (2012).
8. Hui, Y. Y. *et al.* Exceptional Tunability of Band Energy in a Compressively Strained Trilayer MoS_2 Sheet. *ACS Nano* **7**, 7126–7131 (2013).
9. Johari, P. & Shenoy, V. B. Tunable Dielectric Properties of Transition Metal Dichalcogenides. *ACS Nano* **5**, 5903–5908 (2011).
10. Yin, Z. *et al.* Single-Layer MoS_2 Phototransistors. *ACS Nano* **6**, 74–80 (2011).
11. Mak, K. F. *et al.* Tightly Bound Trions in Monolayer MoS_2. *Nat. Mater.* **12**, 207–211 (2013).
12. Bertolazzi, S., Brivio, J. & Kis, A. Stretching and Breaking of Ultrathin MoS_2. *ACS Nano* **5**, 9703–9709 (2011).
13. Pu, J. *et al.* Highly Flexible MoS_2 Thin-Film Transistors with Ion Gel Dielectrics. *Nano Lett.* **12**, 4013–4017 (2012).
14. Castellanos-Gomez, A. *et al.* Elastic Properties of Freely Suspended MoS_2 Nanosheets. *Adv. Mater.* **24**, 772–775 (2012).
15. Lukowski, M. A., Daniel, A. S., Meng, F., Forticaux, A., Li, L. *et al.* Enhanced Hydrogen Evolution Catalysis from Chemically Exfoliated Metallic MoS_2 Nanosheets. *J. Am. Chem. Soc.* **135**, 10274–10277 (2013).
16. Voiry, D. *et al.* Enhanced catalytic activity in strained chemically exfoliated WS_2 nanosheets for hydrogen evolution. *Nat. Mater.* **12**, 850–855 (2013).
17. Huang, X. *et al.* Solution-Phase Epitaxial Growth of Noble Metal Nanostructures on Dispersible Single-Layer Molybdenum Disulfide Nanosheets. *Nat. Commun.* **4**, 1444 (2013).
18. Wang, Q. H., Kalantar-Zadeh, K., Kis, A., Coleman, J. N. & Strano, M. S. Electronics and optoelectronics of two-dimensional transition metal dichalcogenides. *Nat. Nanotech.* **7**, 699–712 (2012).
19. Chhowalla, M. *et al.* The Chemistry of Two-Dimensional Layered Transition Metal Dichalcogenide Nanosheets. *Nat. Chem.* **5**, 263–275 (2013).
20. Xiao, J. *et al.* Electrochemically Induced High Capacity Displacement Reaction of PEO/MoS_2/Graphene Nanocomposites with Lithium. *Adv. Funct. Mater.* **21**, 2840–2846 (2011).
21. Chang, K. & Chen, W. In situ Synthesis of MoS_2/Graphene Nanosheet Composites with Extraordinarily High Electrochemical Performance for Lithium Ion Batteries. *Chem. Commun.* **47**, 4252–4254 (2011).
22. Splendiani, A. *et al.* Emerging Photoluminescence in Monolayer MoS_2. *Nano Lett.* **10**, 1271–1275 (2010).
23. Mak, K. F., He, K., Shan, J. & Heinz, T. F. Control of Valley Polarization in Monolayer MoS_2 by Optical Helicity. *Nat. Nanotech.* **7**, 494–498 (2012).
24. Adachi, S., Capper, P., Kasap, S. & Willoughby, A. *Properties of Semiconductor Alloys: Group-IV, III-V and II-VI Semiconductors* (Wiley, Berlin, 2009).
25. Komsa, H.-P. & Krasheninnikov, A. V. Two-Dimensional Transition Metal Dichalcogenide Alloys: Stability and Electronic Properties. *J. Phys. Chem. Lett.* **3**, 3652–3656 (2012).
26. Li, H. *et al.* Growth of Alloy $MoS_{2x}Se_{2(1-x)}$ Nanosheets with Fully Tunable Chemical Compositions and Optical Properties. *J. Am. Chem. Soc.* **136**, 3756 (2014).
27. Dumcenco, D. O., Kobayashi, H., Liu, Z., Huang, Y.-S. & Suenaga, K. Visualization and Quantification of Transition Metal Atomic Mixing in $Mo_{1-x}W_xS_2$ Single Layers. *Nat. Commun.* **4**, 1351 (2013).
28. Chen, Y. *et al.* Tunable Band Gap Photoluminescence from Atomically Thin Transition-Metal Dichalcogenide Alloys. *ACS Nano* **7**, 4610–4616 (2013).
29. Xi, J., Zhao, T., Wang, D. & Shuai, Z. Tunable Electronic Properties of Two-Dimensional Transition Metal Dichalcogenide Alloys: A First-Principles Prediction. *J. Phys. Chem. Lett.* **5**, 285–291 (2013).
30. Kresse, G. & Hafner, J. Ab Initio Molecular-Dynamics For Liquid-Metals. *Phys. Rev. B* **47**, 558–561 (1993).
31. Kang, J., Tongay, S., Zhou, J., Li, J. B. & Wu, J. Q. Band Offsets and Heterostructures of Two-Dimensional Semiconductors. *Appl. Phys. Lett.* **102**, 012111 (2013).
32. Mar, A., Jobic, S. & Ibers, J. A. Metal-Metal vs Tellurium-Tellurium Bonding in WTe_2 and Its Ternary Variants $TaIrTe_4$ and $NbIrTe_4$. *J. Am. Chem. Soc.* **114**, 8963–8971 (1992).

Acknowledgments

This work was supported by a KAUST CRG grant and computational resources were provided by KAUST HPC. Research reported in this publication was supported by the King Abdullah University of Science and Technology (KAUST).

Author contributions

L.G. performed the calculations together with Q.Z., Y.Z. and Y.C.; L.G. and U.S. wrote the manuscript. All authors discussed the results and commented on the manuscript.

Additional information

Competing financial interests: The authors declare no competing financial interests.

How to cite this article: Gan, L.-Y., Zhang, Q., Zhao, Y.-J., Cheng, Y. & Schwingenschlögl, U. Order-disorder phase transitions in the two-dimensional semiconducting transition metal dichalcogenide alloys $Mo_{1-x}W_xX_2$ (X = S, Se, and Te). *Sci. Rep.* **4**, 6691; DOI:10.1038/srep06691 (2014).